Exploring Sequence/Folding Space: Folding Studies on Multiple Hydrophobic Core Mutants of Ubiquitin

ARTICLE *in* BIOCHEMISTRY · JUNE 2004

Impact Factor: 3.02 · DOI: 10.1021/bi0361620 · Source: PubMed

6 AUTHORS, INCLUDING:

Katherine Stott
University of Cambridge
37 PUBLICATIONS **1,518** CITATIONS

SEE PROFILE

Sophie E Jackson
University of Cambridge
92 PUBLICATIONS **5,362** CITATIONS

SEE PROFILE

Exploring Sequence/Folding Space: Folding Studies on Multiple Hydrophobic Core Mutants of Ubiquitin[†,‡]

Claudia G. Benítez-Cardoza,[§] Katherine Stott,[||] Miriam Hirshberg,[||] Heather M. Went,[§] Derek N. Woolfson,[⊥] and Sophie E. Jackson*[,§]

University of Cambridge, Chemistry Department, Lensfield Road, Cambridge, CB2 1EW, United Kingdom, University of Cambridge, Department of Biochemistry, 80 Tennis Court Road, Old Addenbrookes Site, Cambridge, CB2 1GA, United Kingdom, and University of Sussex, School of Life Sciences, John Maynard-Smith Building, University of Sussex, Falmer BN1 9QG, United Kingdom

Received December 2, 2003; Revised Manuscript Received March 5, 2004

ABSTRACT: The stability, dynamic, and structural properties of ubiquitin and two multiple hydrophobic core mutants were studied. One of the mutants (U4) has seven substitutions in the hydrophobic core (M1L, I3L, V5I, I13F, L15V, V17M, and V26L). On average, its side chains are larger than the wild-type, and it can thus be thought of as having an overpacked core. The other mutant (U7) has two substitutions (I3V and I13V). On average, it has smaller side chains than the wild-type, and it can therefore be considered to be underpacked. The three proteins are well-folded and show similar backbone dynamics (T_1, T_2, and HNOE values), indicating that the regular secondary structure extends over the same residue ranges. The crystallographic structure of U4 was determined. The final R_{factor} and R_{free} are 0.198 and 0.248, respectively, at 2.18 Å resolution. The structure of U4 is very similar to wild-type ubiquitin. Remarkably, there are almost no changes in the positions of the C_α atoms along the entire backbone, and the hydrogen-bonding network is maintained. The mutations of the hydrophobic core are accommodated by small movements of side chains in the core of mutated and nonmutated residues. Unfolding and refolding kinetic studies revealed that U4 unfolds with the highest rates; however, its refolding rate constants are very similar to those of the wild-type protein. Conversely, U7 seems to be the most destabilized protein; its refolding rate constant is smaller than the other two proteins. This was confirmed by stopped-flow techniques and by H/D exchange methodologies. This work illustrates the possibility of repacking the hydrophobic core of small proteins and has important implications in the de novo design of stable proteins.

The de novo design of stable proteins still represents a considerable challenge to protein scientists. One of the most important features of the majority of naturally occurring proteins is a tightly packed and highly ordered hydrophobic core. A nativelike core packing is necessary for designed proteins to be stable, fold, and function, and this can constitute a very significant barrier to progress. Ubiquitin has a well-defined hydrophobic core, which is highly conserved in primary sequence. It is a relatively small protein, 76 residues in length, and its three-dimensional structure has been solved at high resolution (*1*−*2*). This has made ubiquitin an ideal model system for both establishing the factors important in determining its stability (*3*−*12*) and in the development of computational approaches to designing hydrophobic cores (*13*−*17*). In addition, the folding of ubiquitin has been studied extensively using a number of different experimental approaches (*18*−*22*). Recently, the kinetics of folding and unfolding have been measured by conventional methods and compared with those derived from the most slowly exchanging amide residues in native ubiquitin. Rate constants, of folding and unfolding, from these two very different types of experiments showed good agreement (*23*).

Ubiquitin has also been used as a model system to test novel phage-display-based methodologies to select stable folded domains of proteins from libraries (*24*−*25*). In these studies, a mutant of ubiquitin, which did not fold, was initially created and used as the starting point to generate a library of mutants in the N-terminal hydrophobic core. Mutants that were stable were selected using an assay based on the resistance of stable folded proteins to proteolysis (*24*). Analysis of the selectants that survived treatment with protease showed that there was a distinct preference for wild-type sequences. However, some of the selected constructs had a significant number of mutations as compared to the wild-type protein and quite a different composition in the hydrophobic core (*25*). In this paper, we characterize in detail the stability, folding (by two different approaches: stopped-flow fluorescence and H/D exchange methods), dynamic, and structural properties of two of these mutants. One of the mutants (U4) has seven mutations in the hydrophobic core

[†] This work was funded in part by The Royal Society and The Welton Foundation. The Cambridge Centre for Molecular Recognition is supported by the BBSRC. C.G.B.-C. acknowledges partial funding from the CONACyT 010092, DGRI/SEP, and The Welton Foundation.

[‡] The atomic coordinates of U4 have been deposited in the Protein Data Bank, www.rcsb.org [PDB ID code 1SIF].

* To whom correspondence should be addressed. Tel: +44 (0) 1223 762011. Fax: +44 (0) 1223 336362. E-mail: sej13@cam.ac.uk.

[§] University of Cambridge, Chemistry Department.

[||] University of Cambridge, Department of Biochemistry.

[⊥] University of Sussex.

10.1021/bi0361620 CCC: $27.50
Published on Web 04/17/2004

(M1L, I3L, V5I, I13F, L15V, V17M, and V26L). On average, its side chains are larger than wild-type and thus can be thought of as having an overpacked core. The other mutant (U7) has two mutations in the sequence (I3V and I13V). On average, it has smaller side chains than wild-type and therefore can be considered underpacked.

MATERIALS AND METHODS

Materials. Isopropyl β-d-thiogalactopyranoside (IPTG)[1] and analytical grade guanidinium chloride (GdmCl) were purchased from Melford Laboratories Ltd. All other materials were analytical grade and purchased from Sigma.

Expression Vectors. Wild-type and mutant proteins were expressed and purified as described elsewhere (*24*−*25*). The expression vector pCANTABB-WT-UBQ was used for the overexpression of wild-type and mutant proteins. This vector expresses ubiquitin as a fusion with the gIII periplasmic leader sequence-hexahistidine tag LQD-ubiquitin-GLDQQ-pIII. The plasmid has been constructed with two suppressible amber (TAG) codons between ubiquitin gene and pIII; this allows expression of the hexahistidine-tagged ubiquitin without the pIII fusion partner in a nonsuppressor strain of *Escherichia coli* such as HB2151. ^{15}N-labeled proteins were expressed in minimal media containing M9 salts plus supplements (2 mM $MgSO_4$, 1 mM $FeCl_2$, 2.0 mM H_3BO_3, 0.3 mM $CoCl_2$, 4×10^{-2} mM $CuCl_2$, 5 mM $ZnCl_2$, 6.5 mM Na_2MoO_4, 0.4 mM $MnCl_2$, 1 mg L^{-1} each of biotin, choline chloride, folic acid, niacinamide, D-pantothenate, and pyridoxal, 0.1 mg L^{-1} of riboflavin, 5 mg L^{-1} of thiamine, 2.5 mM $CaCl_2$, and 50 mM $ZnSO_4$), 6 g L^{-1} glucose, and 1.5 g L^{-1} $^{15}NH_4Cl$ as the only nitrogen source. Yields of purified wild-type and mutant proteins expressed in rich media were somewhat variable, typically 4−16 mg/L for wild type, 2−8 mg/L for U4, and 1−13 mg/L for U7. Yields of purified proteins expressed in minimal media were not significantly different and were typically 8 mg/L (wild-type), 2−6 mg/L (U4), and 9−11 mg/L (U7).

Stopped-Flow Experiments. An Applied Photophysics Stopped Flow Reaction Analyzer (model SX-18MV) was used, and data were acquired and analyzed using the Applied Photophysics Kinetic Workstation, version 4.099, supplied. The temperature was 15 °C. In all experiments, final buffer concentrations were 50 mM glycine-HCl pH 2.2. Buffers were prepared volumetrically. All stock GdmCl solutions were prepared in volumetric flasks and stored in aliquots at −20 °C until use.

Unfolding Studies. Unfolding was performed by GdmCl jump experiments in the following manner. Unfolding was initiated by diluting one volume of an aqueous protein solution (55 μM in 50 mM buffer) into 10 volumes of concentrated GdmCl solution (containing 50 mM buffer) to give final GdmCl concentrations between 2 and 7.5 M.

Refolding Studies. Refolding was initiated by GdmCl jump experiments. A solution of unfolded protein was generated by denaturing in 50 mM glycine-HCl pH 2.2 containing 5 M GdmCl. Refolding was initiated by mixing one volume of unfolded protein into 10 volumes of a refolding buffer containing 50 mM glycine-HCl pH 2.2 and appropriate amounts of GdmCl to give final concentrations between 0.45 and 3 M. The final protein concentration, after mixing, was 5 μM. Data were fitted to a single-exponential process with a linear drift that included slow proline isomerization phases. Only the fast phase is considered here. It has been shown that the fast, major phase observed (which corresponds to folding and is not limited by proline isomerization) accounts for 80% of the amplitude (*45*). As no rollover is observed in the kinetic chevron plots, it is assumed that transient aggregation does not occur during folding under these conditions.

Data Analysis. Data from the plots of ln k versus denaturant concentration were fit to a two-state model, using eq 1 (*26*)

$$\ln k = \ln(k_F^{H_2O}\exp(-m_{kF}[D]) + k_U^{H_2O}\exp(m_{kU}[D])) \quad (1)$$

where $k_F^{H_2O}$ and $k_U^{H_2O}$ are the rate constants for folding and unfolding in water, respectively, and m_{kF} and m_{kU} are the slopes of the chevron plot for folding and unfolding, correspondingly.

NMR. The ^{15}N-labeled samples were extensively dialyzed against phosphate buffer 20 mM pH 6.0, and D_2O was added to a final concentration of 10% v/v. The final protein concentrations were 1.5, 0.5, and 3.5 mM for wild-type, U4, and U7, respectively. NMR data were collected on a Bruker DRX spectrometer operating at 500 MHz, equipped with a triple resonance HCN probehead and actively shielded z-gradients. Data were collected at a temperature of 288 K, and unless otherwise stated, water suppression was achieved using established flip-back methods, using shaped selective pulses to return water magnetization to the z-axis followed by WATERGATE to purge any remaining transverse magnetization prior to acquisition (*27*). States/TPPI was used for quadrature detection in the indirect dimension. Data were processed using the AZARA suite of programs (*28*).

^{1}H and ^{15}N Assignment. Assignments were made using ANSIG (*29*). Backbone ^{15}N and ^{1}HN nuclei that could not be assigned by comparison with the wild-type data were assigned using 3-D ^{15}N-HSQC-NOESY (*30*) and 3-D ^{15}N-HSQC-TOCSY (*31*) experiments, recorded with 32($t1$) × 100($t2$) × 1024($t3$) complex pairs of data points and spectral widths of 1140($t1$) × 5556($t2$) × 10 000($t3$) Hz. The mixing times were 100 and 67 ms, respectively.

Relaxation Experiments. T_1 and T_2 relaxation times and $\{^1H\}^{15}N$ heteronuclear NOE enhancements were measured at 500 MHz as described by Farrow et al. (*32*), via a series of 2-D ^{15}N HSQC experiments recorded with 128($t1$) × 640($t2$) complex pairs of data points and spectral widths of 2000($t1$) × 10 000($t2$) Hz. The time-points recorded were

[1] Abbreviations: IPTG, isopropyl β-d-thiogalactopyranoside; GdmCl, guanidinium chloride; NMR, nuclear magnetic resonance; HSQC, heteronuclear single quantum correlation; NOESY, nuclear Overhauser effect spectroscopy; TOCSY, total correlation spectroscopy; T_1, $(1/R_1)$ longitudinal relaxation time; T_2, $(1/R_2)$ transverse relaxation time; NOE, nuclear Overhauser effect; HNOE, heteronuclear Overhauser effect; 2-D, two-dimensional; 3-D, three-dimensional; D_2O, deuterium oxide; PEG, poly(ethylene glycol); k_{op}, opening rate; k_{cl}, closing rate; k_{ch}, exchange rate in model peptides; k_{obs}, observed exchange rate; EX1, mechanism of hydrogen exchange in which k_{obs} equals k_{op}; EX2, mechanism of hydrogen exchange in which k_{obs} equals $k_{ch}(k_{op}/k_{cl})$; K_{op}, equilibrium constant for formation of the exchange-competent conformation; k_F^{H2O} and k_U^{H2O} are the rate constants for folding and unfolding in water, respectively, and m_{kF} and m_{kU} are the slopes of the folding and unfolding arm of the kinetic chevron plot, respectively, K_{eq}, equilibrium constant; ΔG_{D-N}, Gibbs energy change of unfolding; $\Delta\Delta G$, change on free energy on mutation; ΔG_{HX}, apparent Gibbs energy change of opening or exchange; T, temperature; R, universal gas constant.

as follows: R_1 (10, 50, 90, 160, 250, 360, 480, 600) ms; R_2 (15.8, 47.5, 79.2, 110.9, 142.6, 174.2, 237.6, 301.0) ms. The $^1H\{^{15}N\}$ heteronuclear NOE enhancements were obtained by recording two 2-D ^{15}N HSQC experiments, one with 3 s of ^1H saturation and one with a delay of the same length.

H/D Exchange Experiments. These experiments were performed in a very similar way as reported before (*23*), with some slight differences, as follows. Wild-type and mutant ubiquitin were first lyophilized and then dissolved in 0.5 mL of D_2O containing 14 mM each of glycine, glycyl−glycine, and potassium phosphate, pH 5.0. Exchange was initiated at the desired pH by adding 0.1 mL of D_2O containing the appropriate amount of NaOD. Final concentrations were 10 mM of each buffer and 0.5−1 mM of protein. The pH values reported herein are for D_2O solutions and have not been corrected for isotope effects. Experimental dead times (time between dissolving protein to the start of data acquisition) were between 5 and 10 min. Exchange was followed in the pH range from 6.5 to 9.2 at 15 °C. H/D exchange rates were measured from the peak intensities in a time series of 2-D ^{15}N HSQC experiments (*33*). The time-scales on which data were acquired varied depending on pH, mutant, and therefore, rate. Typically, 10 ^1H-^{15}N HSQC of 8 scans each were taken initially, then an additional 8−10 spectra of 64 scans each were acquired at longer time points. Samples were incubated in a 15 °C water bath between data acquisition. To interpret the data, we used the two-state model (*34*).

$$\text{Closed (NH)} \underset{k_{cl}}{\overset{k_{op}}{\rightleftharpoons}} \text{Open (NH)} \xrightarrow{k_{ch}} \text{Exchanged (ND)} \quad (2)$$

In this model, the "Closed" conformation is the exchange-incompetent protonated form, and the "Open" conformation is the exchange-competent protonated form of the protein. The two states interconvert with rate constants k_{op} (rate constant of the opening step) and k_{cl} (rate constant of the closing step). Exchange happens only with the open conformation with a rate constant k_{ch}, which is dependent on sequence, temperature, and pH. Values of k_{ch} can be estimated on the basis of model compounds (*35*). Under folding conditions, $k_{cl} \gg k_{op}$, so that the observed rate constant for exchange k_{obs} can be defined as

$$k_{obs} = k_{op}k_{ch}/k_{cl} + k_{ch} \quad (3)$$

Under conditions where k_{ch} is greater than k_{cl}, the observed rate constant of exchange (k_{obs}) becomes k_{op}. This is known as the EX1 regime. On the other hand, if k_{cl} is greater than k_{ch}, then $k_{obs}=K_{op}k_{ch}$, where K_{op} is the equilibrium constant for formation of the exchange-competent conformation. This is known as the EX2 regime.

X-ray Crystallography. Crystals of U4 were obtained at room temperature by the vapor diffusion method from solution containing 22.5 mg mL^{-1} of protein in water, equilibrated against a well containing 31% PEG 4K and 0.05 M citrate buffer, pH 5.6. Crystals grew within 5−6 weeks. Diffraction data were collected at 100 K on RAXIS image plate using our in-house setup. Diffraction data were processed by the program MOSFLM and reduced using CCP4 programs suite (*36*−*37*). Initial phases were calculated by molecular replacement using wild-type protein as a search model (PDB entry 1UBQ). The structure was model-built and refined using the programs O and Refmac5, respectively (*38*−*39*).

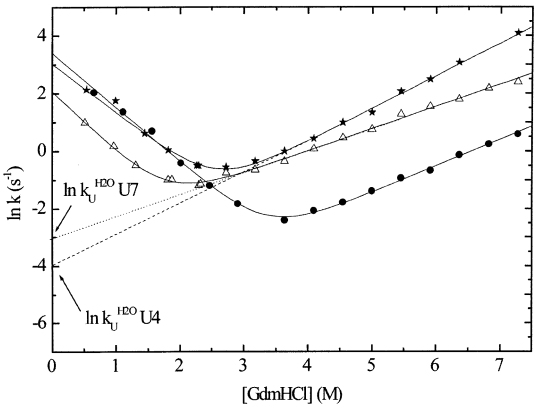

FIGURE 1: Chevron plots showing the unfolding and refolding kinetics of wild-type and mutant ubiquitins at pH 2.2 at 15 °C. Rate constants for unfolding and folding as a function of denaturant concentration for wild-type (filled circles), U4 (stars), and U7 (triangles). The solid lines show the best fit of the data to a two-state model (eq 1). The dashed and dotted lines are extrapolations of the unfolding brain of U4 and U7, respectively.

RESULTS

Kinetic Studies. The unfolding and refolding kinetics of wild-type, U4, and U7 were studied using stopped-flow fluorescence methods. All the kinetic traces are single exponentials in 50 mM glycine, pH 2.2. The unfolding and refolding rate constants at different concentrations of guanidinium chloride were determined for wild-type and mutant proteins. Plots of ln *k* versus denaturant concentration give a chevron, typical of small proteins that fold without significantly populating intermediates states (*26*). Data were fitted to a two-state model using eq 1 (Figure 1). The kinetic parameters obtained from the best fit are summarized in Table 1. From Figure 1 and Table 1, we can see that both mutants are destabilized as compared to wild-type ubiquitin. An equilibrium *m* value, m_{D-N}, can be calculated from the kinetic data and is shown in Table 1. Although the kinetic *m* values vary between wild type, U4, and U7, the equilibrium values are all within experimental error indicating that there are no significant differences in the change in solvent accessible surface area between the native and the denatured states on mutation. Changes in kinetic *m* values can, therefore, be attributed to movements in the position of the transition state on mutation, as indicated by the β-Tanford values also given in Table 1. It is clear that the unfolding rate constants of U4 are slightly higher than those determined for U7. However, the unfolding rate constant in water ($k_U^{H_2O}$) for U4 is 16×10^{-3} s^{-1}, which is slightly smaller than that obtained for U7 (45×10^{-3} s^{-1}). This is due to the larger slope of unfolding (m_{kU}) for U4. The m_{kU} value is a measure of the change in solvent accessible surface area between the native and the transition states. The largest m_{kU} belongs to U4, suggesting that, in this case, the transition state for U4 is less nativelike than for wild-type or U7. Correspondingly, U7 seems to have a slightly more nativelike transition state than wild-type. Changes in m_{kU} values upon mutation have been attributed to movement in the transition state (*40*−*42*) or in extreme cases to a change in the folding pathway (*43*).

Table 1: Kinetic Parameters for the GdmCl-Induced Unfolding and Refolding of Ubiquitin Constructs at 15 °C[a]

construct	$k_F^{H_2O}$ s^{-1}	m_{kF} M^{-1}	$k_U^{H_2O} \times 10^{-3}$ s^{-1}	m_{kU} M^{-1}	ΔG_{D-N} kcal mol^{-1} [b]	m_{D-N} kcal mol^{-1} M^{-1} [c]	β_T
wild-type	30.7 ± 3.2	1.89 ± 0.05	2.5 ± 0.4	0.90 ± 0.03	5.4	1.59 ± 0.03	0.68
U4	23.9 ± 2.3	1.76 ± 0.07	16 ± 2.2	1.12 ± 0.02	4.2	1.64 ± 0.07	0.61
U7	7.8 ± 1.02	2.06 ± 0.13	45 ± 4.4	0.77 ± 0.02	2.9	1.62 ± 0.13	0.73

[a] Values of k_F^{H2O}, k_U^{H2O}, m_{kF}, and m_{kU} were determined from fittings using eq 1. Data were fit only over a denaturant concentration range that shows no curvature. [b] ΔG_{D-N} values were determined as $-RT \ln(k_F^{H2O}/k_U^{H2O})$. [c] $m_{D-N} = RT(m_{kF} + m_{kU})$.

It appears that U4 has a less compact transition state as compared to the wild-type, presumably due to the increase in volume of side chains within the core. As discussed next, a number of the interresidue distances in the core of U4 are reduced as compared to wild-type. Although some of these variations are within the experimental error, there is a general tendency for a more tightly packed core in U4. U4 and wild-type refold with very similar rate constants (Figure 1), implying that the introduction of bulkier residues into the hydrophobic core of ubiquitin does not significantly affect the rate of refolding. On the other hand, U7 refolds approximately three times more slowly than the wild-type, the removal of side chains making favorable interactions in the core destabilizing the transition state suggesting that the N-terminal hydrophobic core region is partially structured in the transition state. The m_{kF} values for the three proteins are very similar, indicating that the three proteins have approximately the same change in surface area buried between the denatured and the transition states.

The equilibrium constants were calculated from $K_{eq} = k_u/k_f$, and they were used to calculate $\Delta G_{D-N} = -RT \ln K_{eq}$. According to the ΔG_{D-N} values, it appears that in the overpacked mutant, U4, the balance between large unfolding and refolding rate constants results in a more stable protein ($\Delta\Delta G = 1.3$ kcal mol^{-1}) as compared to the underpacked mutant, U7 (with only two mutations in the core), which has slightly smaller unfolding rate constants, but its refolding constants are considerably smaller. U7 seems to be the most unstable of the three proteins ($\Delta\Delta G_{D-N} = 2.5$ kcal mol^{-1}).

U4 Structure. To further characterize the impact of multiple core mutations in ubiquitin crystallization, trials were carried out with U4, U7, and wild-type. Efforts to crystallize U7 and wild-type were not successful; however, U4 crystallized readily after 5−6 weeks. The data collection and processing of the U4 X-ray structure are given in Table 2. Initial phases were calculated using molecular replacement with the wild-type structure (PDB entry 1UBQ) modeled built and refined using the programs O and Refmac5, respectively. The final R_{factor} and R_{free} are 0.198 and 0.248, respectively, at 2.18 Å resolution. The final structure of U4 consists of residues 1−71 and 49 water molecules (residues 6, 29, 54, and 63 are only partially observed). The refinement parameters are summarized in Table 3.

Comparison of the U4 and wild-type ubiquitin structures revealed that they are very similar. Remarkably, the backbone conformations are essentially the same with average rmsd of 0.53 Å on C_α atoms. Higher values are observed in the loops, particularly in the loop connecting β4 and the 3_{10} helix (Figures 2 and 3A). Interestingly, the hydrogen-bonding network observed in wild-type ubiquitin is preserved in the mutant. All seven mutations are accommodated by a concerted series of slight movements of the side chains of mutated and nonmutated residues within the core (Figure 3B,C). Several interresidue distances within the core of U4 are smaller as compared to wild-type. Some of the differences are within the experimental error, but the overall trend is for a more tightly packed core. The similarity between U4 and wild-type backbone structures confirms the ability of ubiquitin to tolerate multiple substitutions within the core and to adopt alternatively packed hydrophobic cores, without affecting the overall structure of the protein. Thus, we can confirm that the phage display selection of the hydrophobic core mutants procedure proposed by Woolfson and co-

Table 2: Parameters for the Data Collection and Reduction of the Crystal of U4

detector	Raxis IV++
wavelength (Å)	1.5418
temperature (K)	100
resolution (Å)	2.18
space group	*I*222
cell (Å)	
a	46.81
b	49.03
c	75.86
$\alpha = \beta = \gamma$	90.0
no. of copies in asu	1
reflections collected	48 020
unique reflections	4810
completeness (%)	99.8 (99.4)
multiplicity	4.8 (4.7)
R_{merge} (%)	5.2 (18.2)
I/σ	10.8 (4.6)
Wilson B (Å^2)	28.8

Table 3: X-ray Refinement Statistics

R_{factor} (%)	19.3
R_{free} (%)	24.8
overall *B* value (Å^2)	26.9
no. of protein atoms	560
no. of atoms	49
rms on bond length (Å)	0.023
rms on bond angle (deg)	2.093

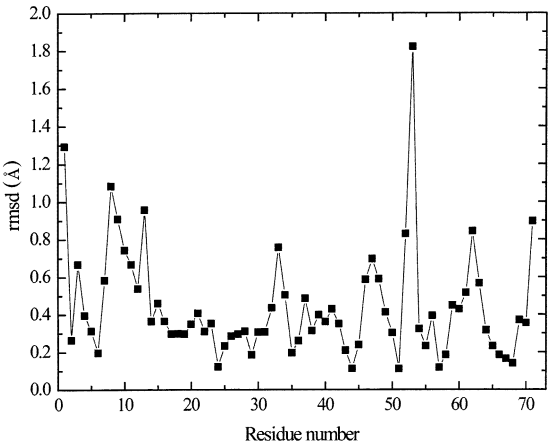

FIGURE 2: C_{alpha} rmsd of the mutant U4 as compared to wild-type ubiquitin as a function of residue number.

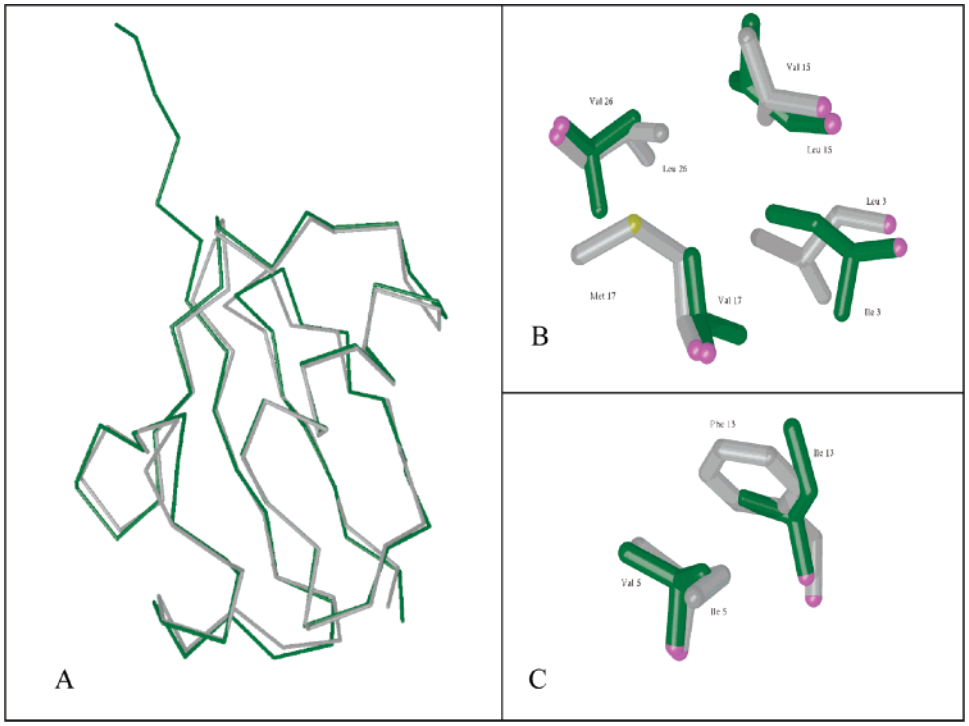

FIGURE 3: Diagrams of the crystallographic structures of wild-type (green) and U4 (grey) ubiquitin. (A) Comparison of the C_α backbones and (B and C) side-chain orientations of the mutated residues in the mutant U4. (B) Residues 3, 15, 17, and 26. (C) Residues 5 and 13 [rendered with the program Bobscript (*54*)].

workers is able to generate alternative core sequences that maintain the backbone structure of the protein (*24*−*25*).

Dynamic Studies. To study the properties of the multiple core mutants in further detail, heteronuclear NMR experiments were undertaken to investigate the effect of mutations on the dynamics and structure of the protein. The three proteins were ^{15}N-labeled and spectra assigned. For the U7 mutant, which has two substitutions, simple comparison of the chemical shifts with those reported for the wild-type protein was sufficient to reassign the mutant spectra. However, for U4, which has seven mutations, it was necessary to perform the assignment from scratch using standard HSQC, NOESY, and TOCSY experiments.

^{15}N-relaxation experiments were used to determine the effect of the mutations on the backbone dynamics. T_1 and T_2 were obtained from a two-parameter fit to a single exponential, and the ^{1}H $\{^{15}$N$\}$ NOE enhancement was obtained from the measured peak heights using the formula I_{sat}/I_{unsat}. T_1, T_2, and NOE values for the three proteins are globally quite similar (Figure 4). The structured regions appear to be maintained despite the mutations, and the unstructured regions (the N- and C-termini and known loop regions) occur in the same residue ranges as in the wild-type and correlate well with other published data on ubiquitin backbone dynamics (*44*). This indicates that all the three molecules are well-folded and highly ordered. However, globally, U4 has similar values for T_1 and T_2 to wild-type, while U7 has slightly higher T_1 and lower T_2 values as compared with wild-type. This is reflected in the correlation times for each protein, which were calculated using T_1/T_2 for the rigid residues, to give 6.2, 6.6, and 6.1 ns for wild-type, U7, and U4, respectively, and are likely to be attributable to large differences in the protein concentration of the samples measured.

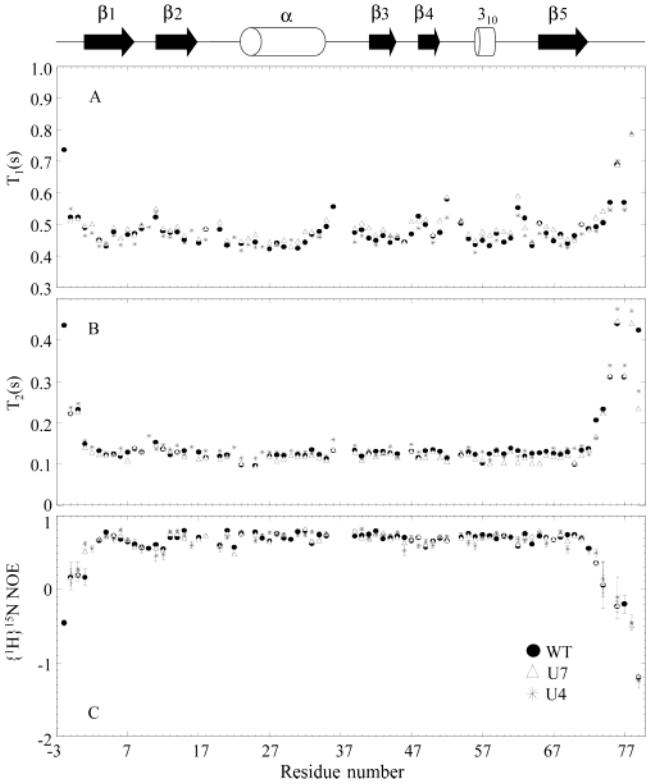

FIGURE 4: Relaxation parameters for wild-type ubiquitin (filled circles), U7 (triangles), and U4 (stars) shown as a function of residue number. (A) Longitudinal relaxation time T_1, (B) transverse relaxation time T_2, and (C) $\{^1$H$\}^{15}$N heteronuclear NOE.

H/D Exchange. To measure the stability and the kinetics of folding and unfolding of the three proteins in the absence of denaturant, H/D exchange experiments were performed over a pH range from 6.5 to 9.2 at 15 °C. Previous studies of amide exchange on ubiquitin have demonstrated that

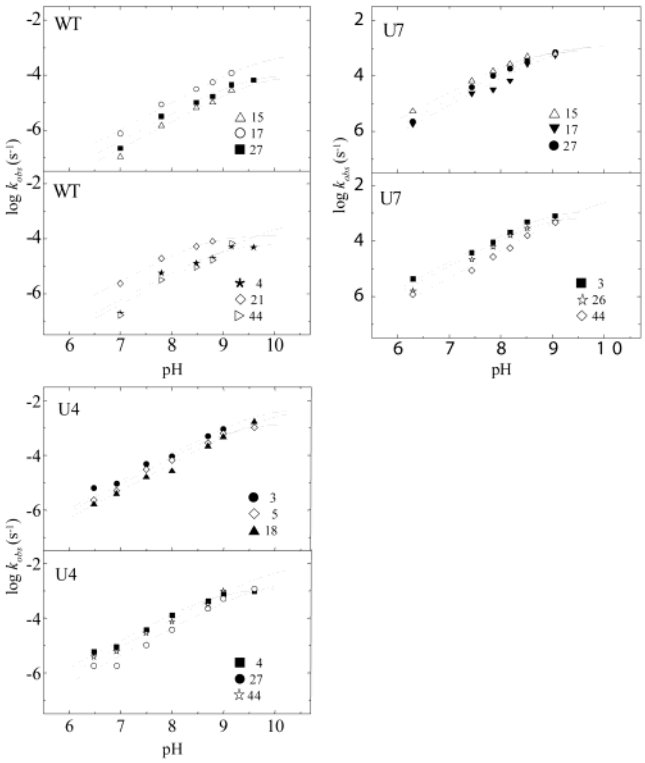

FIGURE 5: pH dependence of the exchange of some of the most slowly exchanging NHs in wild-type ubiquitin, U7 and U4. The symbols indicate the observed rate constants of exchange for the individual residues. The lines are the best fittings according to the simple two-state model, eq 3. For those residues where data in the plateau region were insufficient, simulations of eq 3 were used to obtain the lower limits of k_{op} and k_{cl}.

values of k_{op} and k_{cl} for the most slowly exchanging amide protons in ubiquitin are equivalent to the rate constants for unfolding and folding under native conditions. Also, it has been demonstrated that the stability of ubiquitin does not appreciably change between pH 6.0 and 9.5 (*23*, *45*). Plots of log (k_{obs}) versus pH for the most slowly exchanging NHs in the three proteins are shown in Figure 5. They show clear evidence of EX2 regime for the three proteins at pH <8.5. Above pH 8.5, the pH dependence of k_{obs} decreases, or disappears, for most of the residues, indicating the switch to the EX1 regime. Values of k_{op} and k_{cl} were obtained from nonlinear least-squares fittings with the simple two-state model (eq 3). In those cases where plateau regions were insufficiently defined for fitting, simulations to eq 3 were used to obtain the lower limits for the opening and closing rate constants (*46*). k_{op} and k_{cl} values are summarized in Table 4. k_{op} values cover ranges from 0.7×10^{-4} to 6.1×10^{-4} s^{-1} for wild-type, from 8.2×10^{-4} to 100×10^{-4} s^{-1} for U4, and from 7.7×10^{-4} to 50×10^{-4} s^{-1} for U7. Values of k_{cl} cover wider ranges: from 122 to 1000 s^{-1} for wild-type, from 66 to 1000 s^{-1} for U4, and from 28 to 295 s^{-1} in U7. Consistent with the results obtained in the stopped-flow experiments, the opening rate constants obtained for the individual residues of U4 are slightly larger than those obtained for U7. However, the closing rate constants of U4 are very similar to those obtained for wild-type. The k_{op} and k_{cl} were used to obtain ΔG_{HX}, which is equal to $-RT \ln k_{op}/k_{cl}$. The ΔG_{HX} values obtained are shown in Table 4. The relative stability of the three proteins is consistent with results from stopped-flow experiments at different concentrations of denaturant. Wild-type is the most stable protein, followed by U4, and U7 seems to be the least stable of the three proteins primarily due to the fact that its refolding/closing rate constants are much smaller than for the other two proteins. Despite the different values of thermodynamic and kinetic parameters determined by H/D exchange and stopped-flow fluorescence (it was not possible to perform the stopped-flow experiments under exactly the same conditions as the H/D exchange as there is no change in fluorescence at neutral pH for wild-type ubiquitin (*19*)), the H/D exchange confirms that both mutants are less stable than wild-type. Despite the fact that U4 has seven substitutions within its hydrophobic core as compared to just two for U7, U4 is consistently more similar in refolding/closing rate constants to wild-type. U7 appears to be the least stable protein.

Table 4: Values of k_{op}, k_{cl}, and ΔG_{HX} for Native Wild Type, U4, and U7 at 15 °C[a]

wild type	$k_{op} \times 10^{-3}$ s^{-1}	k_{cl} s^{-1}	ΔG_{HX}[b] kcal mol^{-1}
Ile3	0.11 ± 0.02	335 ± 37	8.5
Phe4	0.07 ± 0.01	122 ± 17	8.2
Val5	0.07 ± 0.01	1001 ± 12	9.4
Leu15	0.1 ± 0.02	242 ± 106	8.4
Val17	0.61 ± 0.17	214 ± 73	7.3
Asp21	0.14 ± 0.02	123 ± 32	7.8
Val26	0.13 ± 0.04	304 ± 177	8.4
Lys27	>0.1[c]	>800[c]	>9.1
Ala28	0.22 ± 0.05	321 ± 153	8.1
Lys29	0.26 ± 0.05	319 ± 111	8.0
Ile30	0.05 ± 0.02	156 ± 6	8.5
Ile44	>0.45[c]	>325[c]	>7.7
	U4		
Leu3	>5.5	>500	>6.5
Phe4	1.21 ± 0.11	70 ± 17	6.3
Ile5	1.53 ± 0.14	93 ± 19	6.3
Val15	1.2 ± 0.16	105 ± 33	6.5
Glu18	>5.0[c]	>1000[c]	>7.0
Leu26	0.82 ± 0.08	66 ± 13	6.5
Lys27	2.08 ± 0.01	429 ± 24	7.0
Ile44	>10.0[c]	>300[c]	>5.9
	U7		
Val3	1.43 ± 0.36	64 ± 30	6.1
Leu15	0.87 ± 0.13	35 ± 12	6.1
Val17	1.44 ± 0.54	59 ± 34	6.1
Glu18	0.77 ± 0.12	28 ± 9	6.0
Asp21	0.78 ± 0.01	91 ± 65	6.7
Val26	0.82 ± 0.08	66 ± 13	6.5
Lys27	1.33 ± 0.17	158 ± 37	6.7
Ile44	>5[c]	>295[c]	>6.3

[a] Values of k_{op} and k_{cl} for all residues (except those marked with *c* were determined from nonlinear regression analysis using eq 3. [b] ΔG_{HX} values were determined as $-RT \ln k_{op}/k_{cl}$. [c] These values were obtained by simulations of eq 3.

DISCUSSION

Methods to Design Hydrophobic Cores. Two methods have previously been used to produce stable hydrophobic core mutants of ubiquitin (*13*, *24*−*25*). In the first approach, a core-repacking algorithm ROC (repacking of cores) was developed and tested. A number of hydrophobic core variants of ubiquitin were designed and characterized using this method (*13*, *16*, *47*). ROC was shown to be a good method to identify alternative core sequences that resulted in proteins with nativelike conformations. In general, cores designed by this method were more stable than randomly designed cores

but less stable than wild-type ubiquitin. One mutant with seven substitutions (1D7) was chosen for further characterization by NMR. This mutant protein showed that the mutations had little impact on the conformation and the backbone dynamics on the milliseconds to picoseconds time scale (*17*). Using an alternative approach, Woolfson and co-workers selected mutants of ubiquitin from a library, which passed through their stability-based selection procedure (*24*−*25*). Variants that survived the proteolytic selection method and were stable showed a clear consensus for the wild-type sequence. All the mutants that were tested were destabilized with respect to wild-type ubiquitin but had melting temperatures within 10 °C. The authors concluded that the core of ubiquitin can accommodate quite large changes and remain well-folded, but the wild-type sequence is near to optimal in terms of stability (*25*). In comparison, other studies have shown that single point mutations (V26I or V26L) can result in an increased stability (*20*). Here, we have chosen two of the stable mutants obtained from the selection method of Woolfson and co-workers (*25*) to characterize in further detail and to establish the effect of multiple mutations within the core of ubiquitin on protein stability, structure, folding, and dynamics. Our results confirm that this selection procedure results in alternative core sequences that maintain the overall structure and backbone dynamics of wild-type ubiquitin. It is interesting to speculate that less-stringent conditions of selection might result in variants with larger differences in stability, structure, and backbone dynamics; or more stringent conditions might lead to more stable and tighter structures.

Identification of Slowly Exchanging Core Residues. It is well-known that exchangeable amide hydrogens that are involved in hydrogen-bonded structure can exchange with solvent deuteriums only when they are transiently exposed to solvent according to eq 2. The most slowly exchanging residues in wild-type ubiquitin that we were able to survey at all the pHs studied were Ile3, Phe4, and Val5, located in the first β-strand; Leu15 and Leu17 situated at the beginning of β2; Asp21 in the loop connecting β2 and α-helix; Val26, Lys27, Ala28, Lys29, and Ile30 all of them in the α-helix; and Ile44 situated in the third β-strand. In contrast, the most slowly exchanging residues observable at all the pHs studied in U4 are Leu3, Phe4, Ile5, Val15, Glu18, Leu26, Lys27, and Ile44, while the positions of the most slowly exchanging amide protons in U7 are Val3, Leu15, Val17, Glu18, Asp21, Val26, Lys27, and Ile44. It is clear that the positions of the slowest exchanging amide protons detectable over the pH range used for wild-type, U4, and U7 differ. For example, some residues, such as residues 4, 5, 17, 21, 28, and 29 have a higher protection in wild-type than in U4 or U7. In contrast, residue 18 has a higher protection in U4 and U7 as compared to wild-type.

Residue 17 in wild-type has the largest (measurable) opening rate constant of all residues, and it also has the second largest opening rate in U7, after residue 44. However, we were not able to observe H/D exchange for residue 17 at any pH for U4. In wild-type and U7, this residue is a valine, while in U4 it is a methionine. Also, we were able to observe residues 21, 28, 29, and 30 for U4 and 4, 5, 28, 29, and 30 for U7 as some of the most slowly exchanging residues in the mutant proteins, only at the lower pHs. At higher pH, their exchange-kinetic curves were too fast to be measurable or reliable. This, in part, may be due to the fact that U4 and U7 unfold faster than the wild-type protein. Interestingly, residue 18 appears to be one of the slowest exchanging amide protons for U4 and U7 but not for wild-type despite the fact that wild-type is the most stable of the three proteins. As mentioned before, the structures of wild-type and U4 are very similar, and the hydrogen-bonding network is not altered by the seven mutations; nevertheless, there are some subtle rearrangements in the hydrophobic core of U4 that allow the side chains of the mutated residues to be accommodated. It is possible that these small movements are responsible for the different protection patterns observed for U4, U7, and wild-type.

Differences in Opening/Unfolding, Closing/Refolding Rate Constants, and $\Delta G_{N-D}/\Delta G_{HX}$ Values as Measured by Stopped-Flow Fluorescence and H/D Exchange. From Tables 1 and 4, it is clear that the values of rate constants and ΔG values obtained by H/D exchange experiments in the absence of denaturant are different to those obtained by the stopped-flow experiments at different concentrations of GdmCl. Unfortunately, a direct comparison cannot be made as the experiments were performed under different solvent conditions. The H/D exchange experiments were measured between a pH range of 6.5 and 9.2, while the stopped-flow experiments were performed at pH 2.2 (it is not possible to measure the kinetics of our constructs at neutral pH by stopped-flow fluorescence; the lack of tryptophan in the proteins leads to undetectable changes in the fluorescence signal under these conditions). Nevertheless, it is known that there are no pH-induced transitions for ubiquitin between pH 1.18 and 8.48 (*48*). In addition, unpublished results from our laboratory (*45*) have shown that the GdmCl-induced denaturation of a F45W variant of ubiquitin measured at pH 2.2, 5.0, and 7.4 is practically independent of pH when measured in GdmCl due to salt effects. Makhatadze and co-workers have shown that charge−charge interactions in ubiquitin stabilize the protein at neutral pH but destabilize the protein under acidic conditions and that these interactions are screened by salts including GdmCl (*3*). Second, the stopped-flow experiments were performed in H_2O while the NMR H/D exchange experiments were performed in D_2O. There are several studies demonstrating that there is only a very minor isotope effects on the kinetics and stability of folding of ubiquitin. For example, Sosnik and co-workers (*11*, *49*) measured the effect of amide isotope substitution by measuring the stability of the protein both with deuterated and with protonated amides, under identical solvent conditions. They found that ubiquitin exhibits only a small isotope effect that is manifested in the unfolding rates. Isotope effects on the stability of ubiquitin were found to be negligible, on the order of 0.10 ×b1 0.02 kcal mol^{-1}. Robertson and co-workers (*23*) have also measured the kinetics of unfolding and folding as a function of denaturant concentration using magnetization transfer at pH 7.0 and 288 K. They found that the k_F value extrapolated to 0.55 M GdmCl in D_2O is equivalent to that determined in 0.55 GdmCl in H_2O at pH 8.5 and 293 K by stopped-flow circular dichroism (*50*). Further, in another study, the denaturation curves of ubiqutin were measured by changes in fluorescence at pH 3 and 298 K with different concentration of GdmCl, in aqueous solvent, and the midpoints of denaturation were consistent with data obtained by titrations monitored by NMR at pH 3.0 in the presence of different concentrations of GdmCl in D_2O at 290

K monitoring the His-68 signal (*51*).

In our case, it is not feasible to compare directly the two different techniques. However, it is known that ΔG_{HX} computed from rate constants for the unfolding mechanism is often, but not always, the same as ΔG for the global denaturation determined by methods such as calorimetry or chemical denaturation. Assuming that the data from calorimetry or chemical denaturation are correct, the simplest explanation for differences in ΔG is that the denatured state retains nonrandom structure around the exchanging amides (*52*). It has been observed that ubiquitin can adopt partially structured states in some conditions (*53*). NMR studies on the partially unfolded A-state of ubiquitin in 60% methanol/40% water, pH 2.0, show nativelike secondary structure for residues 1−33. In addition, it has been reported that wild-type ubiquitin and a designed core variant (1D7) show a number of residues that have protection factors greater than that expected from global stability measurements (*17*). All this supports the existence of nonrandom structure in the unfolded state of wild-type, U4, and U7 variants. It is important to highlight that despite the differences found between the stopped-flow experiments and H/D exchange, the relative stabilities between the three ubiquitin variants studied here are confirmed by the two methodologies. Furthermore, H/D exchange possesses the potential of determining the kinetics and thermodynamics of conformational motions at the residue level under native conditions.

CONCLUSIONS

In summary, the three proteins are well-folded and have very similar backbone dynamics. The overpacked mutant U4 unfolds faster than wild-type but is very similar in structure and refolding rates, despite the presence of seven mutations within its hydrophobic core. U7, the underpacked core mutant that has only two mutations, on the other hand, is the most destabilized of the three proteins. This is reflected in its refolding/closing rate constants, which were considerably smaller than for the other two proteins. This was confirmed by both stopped-flow techniques and by H/D exchange methodologies. This work on ubiquitin illustrates how it is possible to repack the hydrophobic core of small proteins without affecting the structure, folding, or dynamics. It also demonstrates the power of combining libraries with suitable selection methods for generating stable proteins. In addition, the relative refolding and unfolding rates of U4, U7, and wild-type suggest that the N-terminal region of the hydrophobic core is partially structured in the folding transition state of this protein, consistent with results from other protein engineering studies and ϕ-value analysis of ubiquitin (H.M.W. and S.E.J., unpublished results).

ACKNOWLEDGMENT

We thank Michael Finucane who first selected the U4 and U7 mutants.

REFERENCES

1. Vijay-Kumar, S., Bugg, C. E., and Cook, W. J. (1987) Structure of ubiquitin refined at 1.8 Å resolution, *J. Mol. Biol. 194*, 531−544.
2. Vijay-Kumar, S., Bugg, C. E., Wilkinson, K. D., Vierstra, R. D., Hatfield, P. M., and Cook, W. J. (1987) Comparison of the three-dimensional structures of human, yeast, and oat ubiquitin, *J. Biol. Chem. 262*, 6396−6399.
3. Makhatadze, G. I., Lopez, M. M., Richardson, J. M., and Thomas, S. T. (1998) Anion binding to the ubiquitin molecule, *Protein Sci. 7*, 689−697.
4. Ibarra-Molero, B., Loladze, V. V., Makhatadze, G. I., and Sanchez-Ruiz, J. M. (1999) Thermal versus guanidine-induced unfolding of ubiquitin. An analysis in terms of the contributions from charge−charge interactions to protein stability, *Biochemistry 38*, 8138−8149.
5. Loladze, V. V., Ibarra-Molero, B., Sanchez-Ruiz, J. M., and Makhatadze, G. I. (1999) Engineering a thermostable protein via optimization of charge−charge interactions on the protein surface, *Biochemistry 38*, 16419−16423.
6. Thomas, S. T., and Makhatadze, G. I. (2000) Contribution of the 30/36 hydrophobic contact at the C-terminus of the α-helix to the stability of the ubiquitin molecule, *Biochemistry 39*, 10275−10283.
7. Loladze, V. V., Ermolenko, D. N., and Makhatadze, G. I. (2001) Heat capacity changes upon burial of polar and nonpolar groups in proteins, *Protein Sci. 10*, 1343−1352.
8. Loladze, V. V., Ermolenko, D. N., and Makhatadze, G. I. (2002) Thermodynamic consequences of burial of polar and nonpolar amino acid residues in the protein interior, *J. Mol. Biol. 320*, 343−357.
9. Loladze, V. V., and Makhatadze, G. I. (2002) Removal of surface charge−charge interactions from ubiquitin leaves the protein folded and very stable, *Protein Sci. 11*, 174−177.
10. Thomas, S. T., Loladze, V. V., and Makhatadze, G. I. (2001) Hydration of the peptide backbone largely defines the thermodynamic propensity scale of residues at the C′ position of the C-capping box of a-helices, *Proc. Natl. Acad. Sci. 98*, 10670−10675.
11. Shi, Z., Krantz, B. A., Kallenbach, N., and Sosnick, T. R. (2002) Contribution of hydrogen bonding to protein stability estimated from isotope effects, *Biochemistry 41*, 2120−2129.
12. Makhatadze, G. I., Loladze, V. V., Ermolenko, D. N., Chen, X., and Thomas, S. T. (2003) Contribution of surface salt bridges to protein stability: guidelines for protein engineering, *J. Mol. Biol. 327*, 1135−1148.
13. Lazar, G. A., Desjarlais, J. R., and Handel, T. M. (1997) De novo design of the hydrophobic core of ubiquitin, *Protein Sci. 6*, 1167−1178.
14. Lazar, G. A., and Handel, T. M. (1998) Hydrophobic core packing and protein design, *Curr. Opin. Chem. Biol. 2*, 675−679.
15. Lazar, G. A., Johnson, E. C., Desjarlais, J. R., and Handel, T. M. (1999) Rotamer strain as a determinant of protein structural specificity, *Protein Sci. 8*, 2598−2610.
16. Johnson, E. C., and Handel, T. M. (1999) Effect of hydrophobic core packing on side-chain dynamics, *J. Biomol. NMR 15*, 135−143.
17. Johnson, E. C., Lazar, G. A., Desjarlais, J. R., and Handel, T. M. (1999) Solution structure and dynamics of a designed hydrophobic core variant of ubiquitin, *Struct. Fold Des. 15*, 967−976.
18. Briggs, M. S., and Roder, H. (1992) Early hydrogen-bonding events in the folding reaction of ubiquitin, *Proc. Natl. Acad. Sci. 89*, 2017−2021.
19. Khorasanizadeh, S., Peters, I. D., Butt, T. R., and Roder, H. (1993) Folding and stability of a tryptophan containing mutant of ubiquitin, *Biochemistry 32*, 7054−7063.
20. Khorasanizadeh, S., Peters, I. D., and Roder, H. (1996) Evidence for a three-state model of protein folding from kinetic analysis of ubiquitin variants with altered core residues, *Nat. Struct. Biol. 3*, 193−205.
21. Sabelko, J., Ervin, J., and Gruebele, M. (1999) Observation of strange kinetics in protein folding, *Proc. Natl. Acad. Sci. 96*, 6031−6036.
22. Krantz, B. A., and Sosnick, T. R. (2000) Distinguishing between two- and three-state models for ubiquitin folding, *Biochemistry 39*, 11696−11701.
23. Sivaraman, T., Arrington, C. B., and Robertson, A. D. (2001) Kinetics of unfolding and folding from amide hydrogen exchange in native ubiquitin, *Nat. Struct. Biol. 8*, 331−333.
24. Finucane, M. D., Tuna, M., Lees, J. H., and Woolfson, D. N. (1999) Core-directed protein design. I. An experimental method for selecting stable proteins from combinatorial libraries, *Biochemistry 38*, 11604−11612.

25. Finucane, M. D., and Woolfson, D. N. (1999) Core-directed protein design. II. Rescue of a multiply mutated and destabilized variant of ubiquitin, *Biochemistry 38*, 11613−11623.
26. Jackson, S. E., and Fersht, A. R. (1991) Folding of chymotrypsin inhibitor 2. 1. Evidence for a two-state transition, *Biochemistry 30*, 10428−10435.
27. Sklenar, V., Piotto, M., Leppik, R., and Saudek, V. (1993) Gradient-Tailored Water Suppression for ^{1}H-^{15}N HSQC Experiments Optimized to Retain Full Sensitivity, *J. Magn. Reson. A 102*, 241−245.
28. Boucher, W., Department of Biochemistry, University of Cambridge (1993−2002) Cambridge, UK.
29. Kraulis, P. J. (1989) ANSIG: A Program for the Assignment of Protein ^{1}H 2-D NMR spectra by Interactive Graphics, *J. Magn. Reson. 24*, 627−633.
30. Fesik, S. W., and Zuiderweg, E. R. P. (1988) Heteronuclear 3-D NMR spectroscopy−A strategy for the simplification of homonuclear 2-D NMR spectra, *J. Magn. Reson. 78*, 588−593.
31. Zhang, O., Kay, L. E., Olivier, J. P., and Forman-Kay, J. D. (1994) Backbone ^{1}H and ^{15}N resonance assignments of the N-terminal SH3 domain of drk in folded and unfolded states using enhanced-sensitivity pulsed field gradient NMR techniques, *J. Biomol. NMR 4*, 845−858.
32. Farrow, N. A., Muhandiram, R., Singer, A. U., Pascal, S. M., Kay, C. M., Gish, G., Shoelson, S. E., Pawson, T., Forman-Kay, J. D., and Kay, L. E. (1994) Backbone dynamics of a free and phosphopeptide-complexed Src homology 2 domain studied by ^{15}N NMR relaxation, *Biochemistry 33*, 984−1003.
33. Bodenhausen, G., and Ruben, D. J. (1980) Natural abundance nitrogen-15 NMR by enhanced heteronuclear spectroscopy, *Chem. Phys. Lett. 69*, 185−189.
34. Hvidt, A., and Nielsen, S. O. (1966) Hydrogen exchange in proteins, *Adv. Protein Chem. 21*, 287−386.
35. Bai, Y., Milne, J. S., Mayne, L., and Englander, S. W. (1993) Primary structure effects on peptide group hydrogen exchange, *Proteins 17*, 75−86.
36. Leslie, A. G. W. (1992) CCP4 and ESF-EACMB Newsletter on Protein Crystallography, p 26, Daresbury Laboratory, Daresbury, UK.
37. Collaborative Computing Project No. 4. (1994) The CCP4 suite: Programs for protein crystallography, *Acta Crystallogr. D 50*, 760−763.
38. Jones, T. A., Zou, J. Y., Cowan, S. W., and Kjeldgaard S. (1991) Improved methods for building protein models in electron density maps and the location of errors in these models, *Acta Crystallogr. A 47*, 110−119.
39. Winn, M. D., Isupov, M. N., and Murshudov, G. N. (2001) Use of TLS parameters to model anisotropic displacements in macromolecular refinement, *Acta Crystallogr. D 57*, 122−133
40. Matouschek, A., Otzen, D. E., Itzhaki, L. S., Jackson, S. E., and Fersht, A. R. (1995) Movement of the position of the transition state in protein folding, *Biochemistry 34*, 13656−13662.
41. Oliveberg, M., Tan, Y. J., Silow, M., and Fersht, A. R. (1998) The changing nature of the protein folding transition state: implications for the shape of the free-energy profile for folding, *J. Mol. Biol. 277*, 933−943.
42. Otzen, D. E., Kristensen, O., Proctor, M., and Oliveberg, M. (1999) Structural changes in the transition state of protein folding: alternative interpretations of curved chevron plots, *Biochemistry 38*, 6499−6511.
43. Burton, R. E., Huang, G. S., Daugherty, M. A., Calderone, T. L., and Oas, T. G. (1997) The energy landscape of a fast-folding protein mapped by Ala−Gly substitutions, *Nat. Struct. Biol. 4*, 305−310.
44. Tjandra, N., Scott, E., Feller, R. W., and Bax, A. (1995) Rotational diffusion anisotropy of human ubiquitin from 15N NMR relaxation, *J. Am. Chem. Soc. 117*, 12562−12566.
45. *45. Went, H. (2002) Ph.D. Thesis, Protein folding and assembly pathways*, Department of Chemistry, University of Cambridge, Cambridge, UK.
46. Arrington, C. B., and Robertson, A. D. (1997) Microsecond protein folding kinetics from native-state hydrogen exchange, *Biochemistry 36*, 8686−8691.
47. Desjarlais, J. R., and Handel, T. M. (1995) De novo design of the hydrophobic cores of proteins, *Protein Sci. 4*, 2006−2018.
48. Lenkinski, R. E., Chen, D. M., Glickson, J. D., and Goldstein, G. (1977) Nuclear magnetic resonance studies of the denaturation of ubiquitin, *Biochim. Biophys. Acta 494*, 126−130.
49. Krantz, B. A., Moran, L. B., Kentsis, A., and Sosnick, T. R. (2000) D/H amide kinetic isotope effects reveal when hydrogen bonds form during protein folding, *Nat. Struct. Biol. 7*, 62−71.
50. Gladwin, S. T., and Evans, P. A. (1996) Structure of very early protein folding intermediates: new insights through a variant of hydrogen exchange labeling, *Fold Des. 1*, 407−417.
51. Chen, P. Y., Gopalacushina, B. G., Yang, C. C., Chan, S. I., and Evans, P. A. (2001) The role of a β-bulge in the folding of the β-hairpin structure in ubiquitin, *Protein Sci. 10*, 2063−2074.
52. Li, R., and Woodward, C. (1999) The hydrogen exchange core and protein folding, *Protein Sci. 8*, 1571−1590.
53. Stockman, B. J., Euvrard, A., and Scahill, T. A. (1993) Heteronuclear 3-D NMR spectroscopy of a partially denatured protein: the A-state of human ubiquitin, *J. Biomol. NMR 3*, 285−296.
54. Esnouf, R. M. (1997) An extensively modified version of MolScript that includes greatly enhanced coloring capabilities, *J. Mol. Graph. Model. 15*, 132−134.
55. Woolfson, D. N. (2001) Core-directed Protein Design, *Curr. Opin. Struct. Biol. 11*, 464−471.56.
56. Harding, M. M., Williams, D. H., and Woolfson, D. N. (1991) Characterization of a Partially Denatured State of a Protein by 2-Dimensional NMR−Reduction of the Hydrophobic Interactions in Ubiquitin, *Biochemistry 30*, 3120−3128.
57. Cox, J. P. L., Evans, P. A., Packman, L. C., Williams, D. H., and Woolfson, D. N. (1993) Dissecting the Structure of a Partially Folded Protein−Circular Dichroism and Nuclear Magnetic Resonance Studies of Peptides from Ubiquitin, *J. Mol. Biol. 234*, 483−492.

BI0361620